Slow dynamics and field-induced transitions in a mixed-valence oxide solid solution

M. Charilaou, J. F. Löffler, and A. U. Gehring

Phys. Rev. B **83**, 224414 — Published 22 June 2011

DOI: 10.1103/PhysRevB.83.224414

Slow dynamics and field-induced transitions in a mixed-valence oxide solid solution

M. Charilaou,[1,2,*] J. F. Löffler,[2] and A. U. Gehring[1]

[1] *Institute of Geophysics, Department of Earth Sciences, ETH Zurich, Sonneggstrasse 5, 8092 Zurich, Switzerland*

[2] *Laboratory of Metal Physics and Technology, Department of Materials, ETH Zurich, Wolfgang-Pauli-Strasse 10, 8093 Zurich, Switzerland*

(Dated: May 4, 2011)

In this study the spin-glass-like properties of (x)$FeTiO_3$–(1-x)Fe_2O_3, with $x = 0.8$ and 0.9, as prominent mixed valence state solid solution, were investigated by means of *ac* susceptibility and *dc* magnetization measurements. Dynamic *ac* susceptibility indicates freezing at finite temperature T_f, obeying a power law with a dynamic exponent $z\nu \approx 7$, close to that of the 3D Ising spin-glass, and relaxation rates in the kHz-range. The slow dynamics are explained by the presence of ordered superspins, whose relaxation rate decreases with increasing superspin size. In the frozen state, symmetry breaking is observed at a critical field H_{cr} which decreases with temperature obeying a power law $H_{cr}^{2/3} \propto T$, and is followed by a metamagnetic transition with increasing field similar to that of the end-member $FeTiO_3$, obeying a $H_{cr}^{3/2} \propto T$ law. The two transitions converge near the freezing temperature, thus denoting the $H - T$ phase diagram of the system.

PACS numbers: 75.30.Et, 75.40.Gb, 75.47.Lx, 75.50.Lk, 64.60.Ht

Keywords: hemo-ilmenite, spin-glass, frustration, critical slowing down, symmetry breaking

I. INTRODUCTION

Disorder, magnetic frustration, and spin-glass behavior have been studied extensively in the past decades[1–6]. A variety of such spin-glass systems has been investigated experimentally and valuable, often system-specific information has been gained over the years. Among the synthetic systems there is one mixed valence state oxide solid solution that has a naturally occurring equivalent: the hemo-ilmenite solid solution series $(x)FeTiO_3$-$(1\text{-}x)Fe_2O_3$ is an important magnetic carrier in fast-cooled rock bodies in the Earth's crust and can cause long-wavelength magnetic anomalies[7–10]. Moreover, different members of this series have been used for thermometry in order to constrain physical chemical conditions to infer geological processes in the crust[11,12]. Synthetic[13–18] and natural[19,20] solid solutions with $x > 0.6$ exhibit a characteristic spin-glass-like freezing at low temperature ($T < 40$ K). In a geological context this intrinsic property has a strong potential to detect ilmenite-rich solid solutions in rock samples. Although this property has been investigated both experimentally[13–20] and theoretically[21] the mechanism behind the spin-glass freezing still remains unclear. In this paper we therefore present an extensive experimental investigation at low temperature in order to elucidate the spin-glass state of the hemo-ilmenite solid solution.

Both end-members are antiferromagnetic, with Néel temperature $T_N = 58(1)$ K for ilmenite $FeTiO_3$ ($R\bar{3}$), and 950(5) K for hematite $\alpha-Fe_2O_3$ ($R\bar{3}c$). The solid solution is a large band-gap semiconductor and exhibits ferrimagnetic ordering for compositions $0.5 < x < 0.95$, and is antiferromagnetic for $0 \leq x \leq 0.5$. The ordering temperature of the solid solution and the transition from $R\bar{3}c$ to $R\bar{3}$ symmetry is a linear function of the composition x[18,22,23]. In the $R\bar{3}$ symmetry, Fe(II) and Ti(IV) ions are ordered in alternating layers and the Fe(III) ions are distributed evenly in the unit cell, whereas in the $R\bar{3}c$ symmetry there is no preferential ordering and all cations are distributed evenly in the unit cell[22]. This distribution of cations of different valence states creates charge imbalances, which are evened out at the octahedral O_6 faces by means of charge sharing. This leads to lattice distortions along the c–axis and in the basal planes which affect the magnetic ordering of the solid solution. This results in a single-ion anisotropy which differs from site to site and generates frustration.

The frustration in the solid solution is manifested in a spin-glass-like freezing at low temperature for the composition range $0.60 < x < 0.95$[13]. Pioneering work was published by Ishikawa et al.[13,14], who postulated that the spin-glass behavior of the hemo-ilmenite changes from cluster spin-glass above the percolation threshold ($x \approx 0.83$) to reentrant spin-glass below it. Although it is intuitively deducible that the spin-glass-like state is due to the competing Fe(II)–Fe(III) interactions, the freezing 'transition' is still not well understood and the behavior of the system in the frozen state remains unclear. Therefore, in order to provide more insight into the mechanisms of the spin-glass freezing, we fabricated two solid solutions with composition $x = 0.8$ and 0.9, and investigated the thermodynamics of the magnetic ordering. Dynamic study of the freezing and investigation of hysteretic effects was performed by means of *ac* susceptibility. The static properties of the magnetic structure above and below the spin-glass freezing were investigated by *dc* magnetization measurements to determine the $H - T$ phase diagram of the solid solution.

II. THEORETICAL CONSIDERATIONS

The *ac* susceptibility $\chi(T)$ is a powerful tool in investigating thermal activation effects, such as freezing processes, because it probes the dynamic response of the system. Hysteretic effects due to domain-wall movements result in a time delay between field and signal[24] which is manifested in the out-of-phase component of the susceptibility $\chi''(T)$, which is proportional to the energy dissipation[25]. Therefore, the dependence of $\chi''(T)$ on the amplitude of the driving field H_{ac} can be used to detect the change in hysteretic behavior with temperature and determine the transition from ferrimagnetic to spin-glass, which is characterized by a peak of $\chi''(T)$ at the freezing temperature T_f[19,20].

With this in mind, the freezing process can be further studied by means of the frequency dispersion of T_f. Shifting of the transition temperature with frequency is a typical feature of thermal activation processes, such as spin-glass freezing or superparamagnetic blocking. In spin glasses the frequency dispersion is due to the change of relaxation rates with temperature, which are expected to slow down[26,27]. This can be described using a dynamic scaling law[26–29]:

$$\omega = \omega_0 \left(\frac{T_f(\omega) - T_f}{T_f} \right)^{z\nu}, \tag{1}$$

where $T_f(\omega)$ is the freezing temperature at frequency ω, ω_0 is an intrinsic constant related to the relaxation rate (but not the actual rate), and $z\nu$ is the dynamic exponent[29,30]. This exponent is the product of the critical exponent ν for the coherence length ξ, which diverges at the freezing temperature with ξ^ν, and the dynamic exponent z, which relates the relaxation time to the coherence length with[30,31] $\tau \propto \tau_0 \xi^z$.

In addition, the freezing temperature T_f is predicted to shift when an external static field is superimposed, following the so-called de Almeida-Thouless (AT) line[32]. The AT-line separates a non-ergodic (spin-glass-like) phase from an ergodic (paramagnetic) phase in the $H-T$ plane and may be described by the power law[32–34]:

$$H^2 \propto (1 - T/T_f)^3. \tag{2}$$

The existence of the AT-line is a controversial topic in the spin-glass community[33,34]. Most measurements were performed by superimposing a *dc* field on the system during cooling which can shift the freezing temperature[35]. For $Fe_{0.5}Mn_{0.5}TiO_3$, similar to hemo-ilmenite solid solution, such a transition was absent[36]. This kind of experiments on multi-component systems such as hemo-ilmenite can generate complications because the external field pins part of the magnetic structure and subsequently influences the measurement process. In this study another approach is presented where the line of transitions is scanned at constant temperature below T_f under a sweeping field, which is expected to break the spin-glass symmetry. Therefore we attempt to determine the $H-T$ phase diagram of hemo-ilmenite by measuring virgin lines at different temperatures below T_f.

III. EXPERIMENTAL DETAILS

Solid solutions were synthesized by means of solid oxide reaction using high-purity ilmenite $FeTiO_3$ (99.98%) and hematite Fe_2O_3 (99.99%) powders (Alpha Aesar, Germany) . The powders were weighed to mol percentage, mixed with an agate mortar, dried in air at 500 K, and pressed into pellets with a pressure of 80 MPa. The pellets were placed on an Al_2O_3 substrate in silica tubes, which were flushed with Ar gas and sealed with a pressure adjusted to reach 1 atm at 1400 K. The tubes were then heated in a radiation furnace at 1400 K for 50 hrs and then quenched in water. The crystalline structure of the final products was investigated by means of powder X-ray diffraction (XRD) in a Phillips PW1200 diffractometer, using Cu K_α radiation with $\lambda = 1.5405$ Å. Diffraction patterns were recorded in the 2θ angle range between 20° and 90° with a step size of 0.01°. A soller slid of 0.04° was used for better resolution.

Magnetic characterization was performed with a Quantum Design Physical Property Measurement System (PPMS), which operates a superconducting solenoid magnet with field capability of up to 90 kOe, equipped with the *ac*/*dc* magnetometry option ACMS. The instrument allows high-precision measurements with an accuracy of 10^{-7} emu in *ac* and 10^{-5} emu in *dc* mode[37]. The *ac* susceptibility was recorded at 1 kHz with amplitude 5 Oe from 300 K down to 5 K in order to determine the Curie temperature of each sample and ensure that no other phases with magnetic ordering are present. Detailed susceptibility measurements were performed in the range 10 K to 60 K with increasing amplitude from 1 Oe to 14 Oe and at frequencies between 1 Hz and 10 kHz, in order to investigate the field and frequency dependence of the freezing. Magnetization loops were recorded in a field range of ± 15 kOe with a field sweep rate of 10 Oe/s, at temperatures 5 K $< T <$ 60 K.

IV. RESULTS AND DISCUSSION

A. Structure and magnetic ordering

In this study hemo-ilmenite solid solutions with compositions $x = 0.8$ and 0.9 are named as HI80 and HI90, respectively. As a reference for structure determination pure ilmenite (HI100) was used, following the same experimental protocol. The XRD pattern exhibits that the ilmenite $R\bar{3}$ symmetry is evident for both solid solutions, as is expected for quenching from 1400 K[22]. All peaks can be indexed according to the rhombohedral (hexagonal) hemo-ilmenite structure (Fig. 1). The absence of additional peaks suggests no impurity contents within the empirical 3% detection limit of XRD. Rietveld refinement shows, based on the difference between the calculated and the measured patterns $I_{obs} - I_{fit}$, that disorder is evident in the structure along the *c*-axis but also in the basal planes. As discussed in Sec. I, this disorder in hemo-ilmenite originates from the charge imbalance between Fe(III) and Fe(II)-Ti(IV) and the subsequent lattice distortions. The randomness of the Fe(III)-ion positions in the $R\bar{3}$ symmetry, and therefore of the local distortions, permits no quantitative considerations but only a statistical description, which is reflected in the quality of the profile fitting. The weighted profile values R_{wp} are a measure of the agreement between fitted (I_{fit}) and observed data (I_{obs}): $R_{wp} = \sqrt{\sum W\left(I_{fit} - I_{obs}\right)^2 / \sum W I_{obs}^2}$, where W is a weighting factor. These factors lie in the range of 14% – 17%, the smallest being that for ilmenite. The fit quality decreases with increasing Fe(III) content due to enhencement of lattice distortion. The R_{wp} values and the lattice constants are listed in Table I.

The unit cell volumes V_{uc} calculated from the lattice constants are used to deduce the composition of the end-products[38] (Table I). The values obtained for HI80 and HI90 agree well with those reported in literature[21,38].

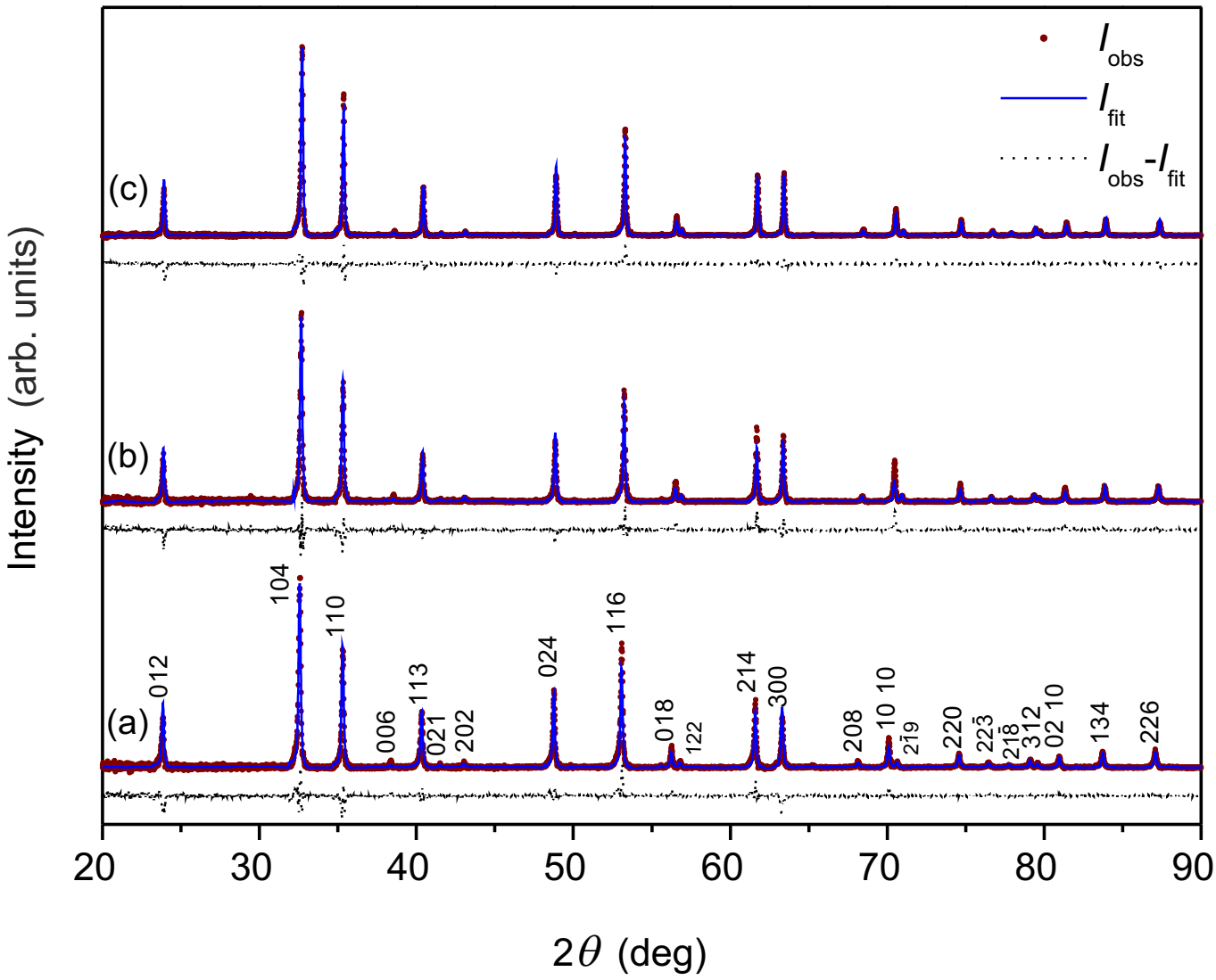

FIG. 1. X-ray diffraction patterns for samples HI80 (a), HI90 (b) and HI100 (c). Dots represent measured data $I_{\rm obs}$, solid lines represent fitted patterns $I_{\rm fit}$, and dotted lines represent the difference $I_{\rm obs} - I_{\rm fit}$.

TABLE I. Lattice constants a and c, unit cell volumes $V_{\rm uc}$, weighted profile fit parameters $R_{\rm wp}$, and Curie temperatures $T_{\rm C}$ for HI80, HI90, and HI100.

x	a [Å]	c [Å]	$V_{\rm uc}$ [Å^3]	$R_{\rm wp}$ [%]	$T_{\rm C}$ [K]
0.80	5.081(2)	14.010(2)	313.28(5)	16.7	227(1)
0.90	5.084(2)	14.021(2)	313.99(5)	14.9	143(1)
1.00	5.089(2)	14.082(2)	316.09(5)	14.4	58(1)

Compared to $V_{\rm uc}$, the Curie temperature $T_{\rm C}$ of the solid solution is a much more reliable index to infer composition because it changes by 9 K per mol% ilmenite, in contrast to $V_{\rm uc}$, which changes by only 0.14 Å^3. Considering the experimental uncertainties with 0.05 Å^3 for $V_{\rm uc}$ and 1 K for $T_{\rm C}$, the latter is more accurate. The Curie temperature $T_{\rm C}$ of the samples determined by ac susceptibility at the onset of the $\chi''(T)$ component of the susceptibility upon cooling, where hysteretic effects first appear at the ordering[24]. The $T_{\rm C}$ of the the solid solutions are indicated by arrows in Fig. 2(a) and listed in Table I. The obtained values for $T_{\rm C}$ are in good agreement with the starting composition of the solid solution.

B. Dynamic susceptibility

In a first step the exact freezing temperature T_f was determined by investigating the hysteretic behavior upon cooling using the amplitude dependence of the imaginary part of the susceptibility χ'' (see Fig. 2(b)).

The characteristic peak of χ'' occurs at T_f, which is more accurately determined by using the derivative of the susceptibility $\mathrm{d}\chi''(T)/\mathrm{d}T$, which becomes zero at T_f (Fig. 2(b)). The field dispersion $\chi''(H_{ac})$ provides more information. Above the freezing temperature the field dispersion is parabolic, which indicates the energy dissipation due to the rotation of domain magnetization vectors in the ferrimagnetic structure[24,25]. Upon cooling the field dispersion becomes narrower and at the center of the characteristic peak χ'' becomes linear, i.e. $\chi''(T) \propto H_{ac}$ (Fig. 2(b)). The linear behavior with H_{ac} indicates that domains are smeared out with freezing. Below the freezing point less energy is dissipated (because no magnetization rotation takes place), which results in a decrease of $\chi''(T)$ with decreasing temperature.

With increasing frequencies, T_f is shifted to higher temperatures and the χ'' peak becomes wider (Fig. 3). The width of the χ'' peak is an index for the distribution of relaxation times, and the fact that it gets narrower for low frequencies, i.e. for lower temperatures, suggests a convergence of relaxation times with decreasing temperature, consistent with critical slowing down. Fig. 3 shows the frequency dispersion of the freezing temperature for samples HI80 and HI90. The data for both samples can be fitted to the power law describing critical slowing down using equation 1 (Fig. 3). The three-parameter fit needs to be performed iteratively in order to avoid reciprocative over- or under-estimations of the parameters. The best fit is given with values of $T_\mathrm{f} = 18(2)$ K and $z\nu = 8(1)$ for HI80, and $T_\mathrm{f} = 22(1)$ K and $z\nu = 7(1)$ for HI90. The values for ω_0 lie in the range of a few kHz (30(10) kHz) and are quite low considering typical GHz rates for spin glasses determined in the Néel formulation. However, attempting to use an Arrhenius activation law (Néel equation), which assumes no transition at finite temperature, does not adequately describe the data. The fits using Eq. 1 produce finite freezing temperatures for both solid solutions, which points to an actual transition. The dynamic exponents are also very close to the theoretical value of 6(1) for the 3D Ising spin glass[29]. The Ising-like behavior of the system has been confirmed and investigated extensively in Ref.[21].

Moreover, the discrepancy of the low relaxation rates can be reconciled by the following scenario: values for ω_0 in the GHz range, usually found for spin glasses, correspond to thermal fluctuation rates of single spins, which, in turn, corresponds to paramagnetic-like behavior above T_f[30]. However, in the case of an ordered magnetic structure, such as ferrimagnetic hemo-ilmenite, the thermal fluctuations occur by collective flipping of coupled spins, i.e., of a superspin[30,39], whose size can be defined by the number of single spins N it comprises. The energy barrier that a superspin has to overcome during each collective flip is approximately N–times larger than the barrier of the single-spin flip. Hence the thermal fluctuation rate, i.e., the relaxation, of the collective flipping decreases with increasing superspin size according to $\omega \propto \exp(-NE_a/k_\mathrm{B}T)$, where E_a the energy barrier of a single-spin flip.

Considering superspins, it can be assumed that they define the coherence length ξ instead of single spins, i.e., lattice sites. Therefore, when $\xi = 1$ the correlation lies at the dimension of the superspin and contains N lattice sites. With this in mind, when the frequency of the *ac* measurement is comparable to ω_0, as found for this system, ξ is very close to 1.

The comparison between HI80 and HI90 indicates no distinctive freezing processes, i.e. as proposed for reentrant and cluster spin-glass by Ishikawa[14]. However, there is a minor deviation of process parameters, such as the dynamic exponent $z\nu$ and freezing temperature T_f, which is probably an effect of increasing Fe(III) in the system.

C. Static *dc* magnetization

In order to study the static behavior of the spin-glass-like state we performed *dc* magnetization measurements. Fig. 4 shows the virgin lines $m(H)$ and the *dc* susceptibility $\mathrm{d}m(H)/\mathrm{d}H$ for HI90 at two temperatures below T_f. For small applied fields the magnetic moment increases linearly with the applied field H up to a *critical field* H_cr where the *dc* susceptibility $\mathrm{d}m(H)/\mathrm{d}H$ exhibits a peak. Within the field range up to H_cr the curve is fully reversible, indicating the symmetry in the glassy state. At H_cr the magnetic moment increases abruptly and hysteretic effects appear, which indicate a breaking of the symmetry. At $T = 5$ K, only one transition at around 5.5 kOe is visible. At $T = 15$ K, however, two transitions are found: one at around 1 kOe and the other at 3 kOe. The $m(H)$ curve becomes irreversible after the transitions pointing to the onset of order. When the external field is removed, the remanent moment relaxes with time and obeys a power law $m_\mathrm{R}(t) = At^{-z}$ (data not shown), similar to that observed for $Mn_{0.5}Fe_{0.5}TiO_3$[40]. This suggests that, although order can be induced by the external field after a long enough period of time, the system may eventually relax and reach the glassy pseudo-ground state again. The reentry in the glassy state can also be forced by gradually demagnetizing the system with the external field which is slowly oscillated with decreasing amplitude down to zero. After this process the virgin lines exhibit the same behavior as they do in the initial condition.

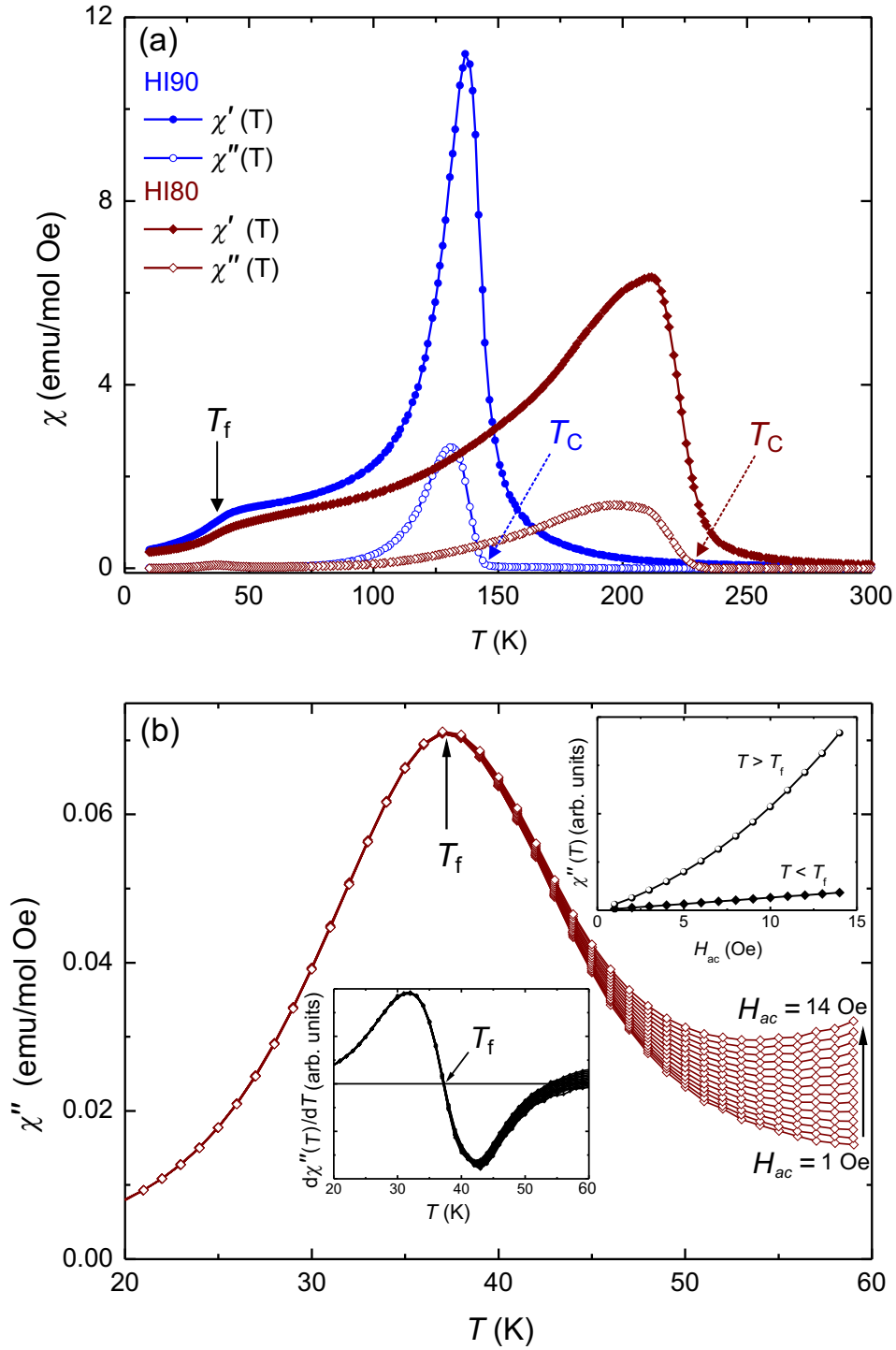

FIG. 2. (a) In- (full symbols) and out-of-phase component (hollow symbols) of the *ac* susceptibility for HI90 and HI80 indicating the Curie $T_{\rm C}$ and freezing temperature $T_{\rm f}$, measured at 1 kHz with a driving field amplitude of 5 Oe. (b) Out-of-phase susceptibility $\chi''(T)$ of the HI80 sample measured at different field amplitudes H_{ac} varying from 1 to 14 Oe at 1 kHz. Upper right inset shows the field-dispersion of $\chi''(T)$ above (circles) and below (diamonds) the freezing temperature $T_{\rm f}$. Lower middle inset shows the determination of the exact freezing point by using the derivative of the susceptibility $\mathrm{d}\chi''(T)/\mathrm{d}T$.

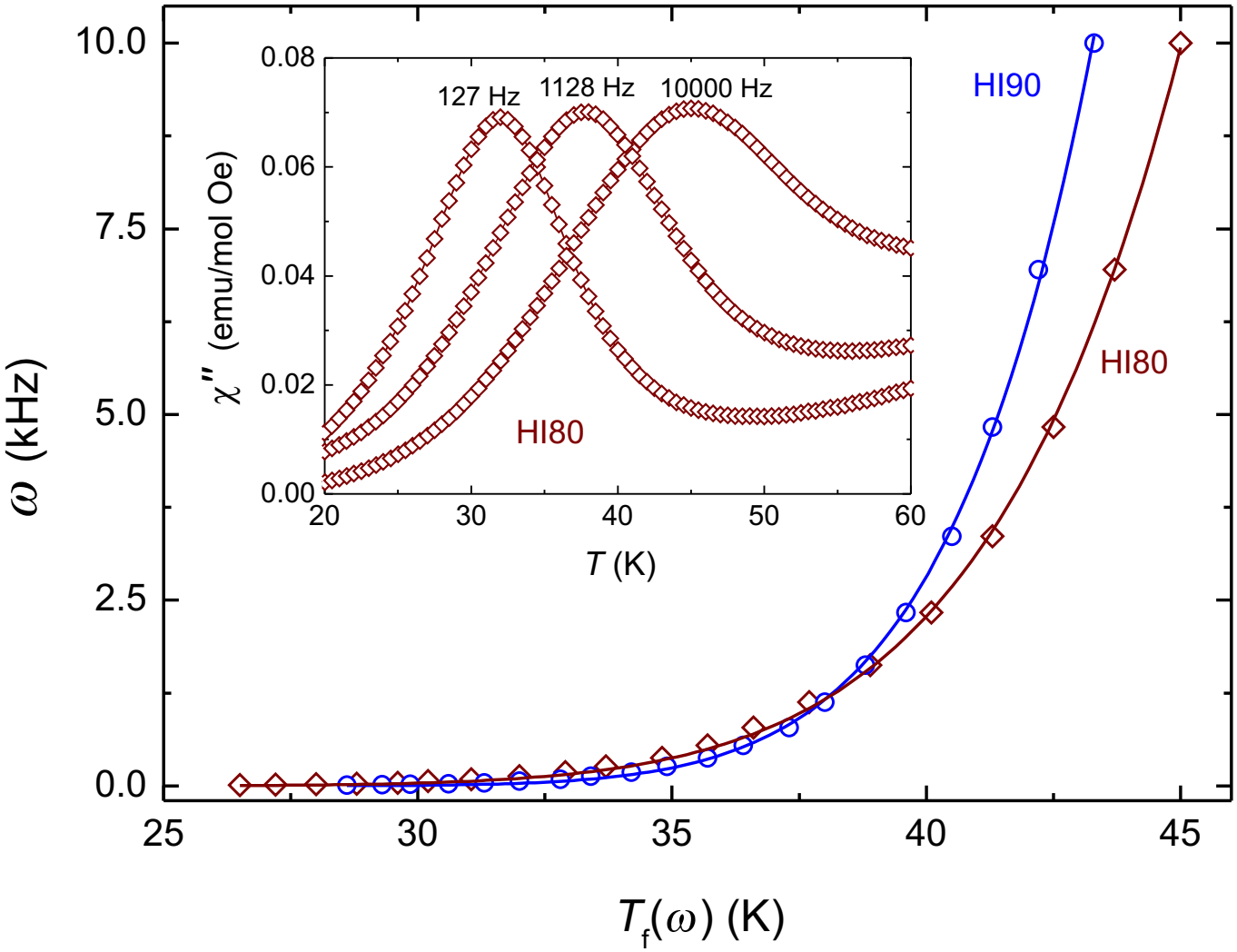

FIG. 3. Frequency dispersion of the freezing temperature $T_f(\omega)$ determined from the out-of-phase susceptibility component $\chi''(T)$ for HI80 and HI90 with driving field amplitude $H_{ac} = 10$ Oe. Solid lines correspond to fits using a dynamic scaling power-law (see Eq.1). The inset shows the $\chi''(T)$ of HI80 for three different frequencies as indicated in the figure.

The temperature evolution of the two transitions shows immediately that they are of different nature (Fig. 5). The low-field and high-field transitions can be identified separately only below a threshold value of approximately 25 K. Above this point the two transitions merge, and disappear upon warming (see closed circles in Fig. 5). The threshold value of about 25 K is in reasonable agreement with the value of T_f determined by *ac* susceptibility. The occurrence of this transition above T_f demonstrates that frustration is evident for temperatures higher than the actual T_f, and can be interpreted as the ordering of the Fe(II). Moreover, at low temperature ($T < 5$ K) the transition takes place at a higher field $H > 5.5$ kOe and shows a discontinuity at around 6 K. This suggests a merging of the two transitions into one single event with decreasing temperature. A field-induced symmetry breaking and a transition from spin glass to paramagnetic was expected according to the AT-line, as discussed in Sec. II. However, the occurrence of two field-induced transitions yields information that is system-specific for hemo-ilmenite.

We find that the critical field of the low-field transitions can be described by the power law for the AT-line (Fig. 5). The high-field transition obeys another power law, $H \propto (1-T/T_f)^{2/3}$, and indicates a metamagnetic transition similar to that of ilmenite[41] (see inset of Fig. 5). The thermodynamic behavior of the metamagnetic transition indicates that the process is governed by the inter-layer exchange interaction[41]. The dramatic drop of the critical field (85 kOe for $FeTiO_3$ to 6 kOe for the solid solution) is a result of the dilute presence of Fe(II) and Fe(III) in the lattice: due to their different modulation lengths along the *c*–axis[42] the uniaxiality of the layered structure is strongly reduced. The symmetry-breaking and the metamagnetic transition may therefore be attributed to the Fe(III) and Fe(II) ions,

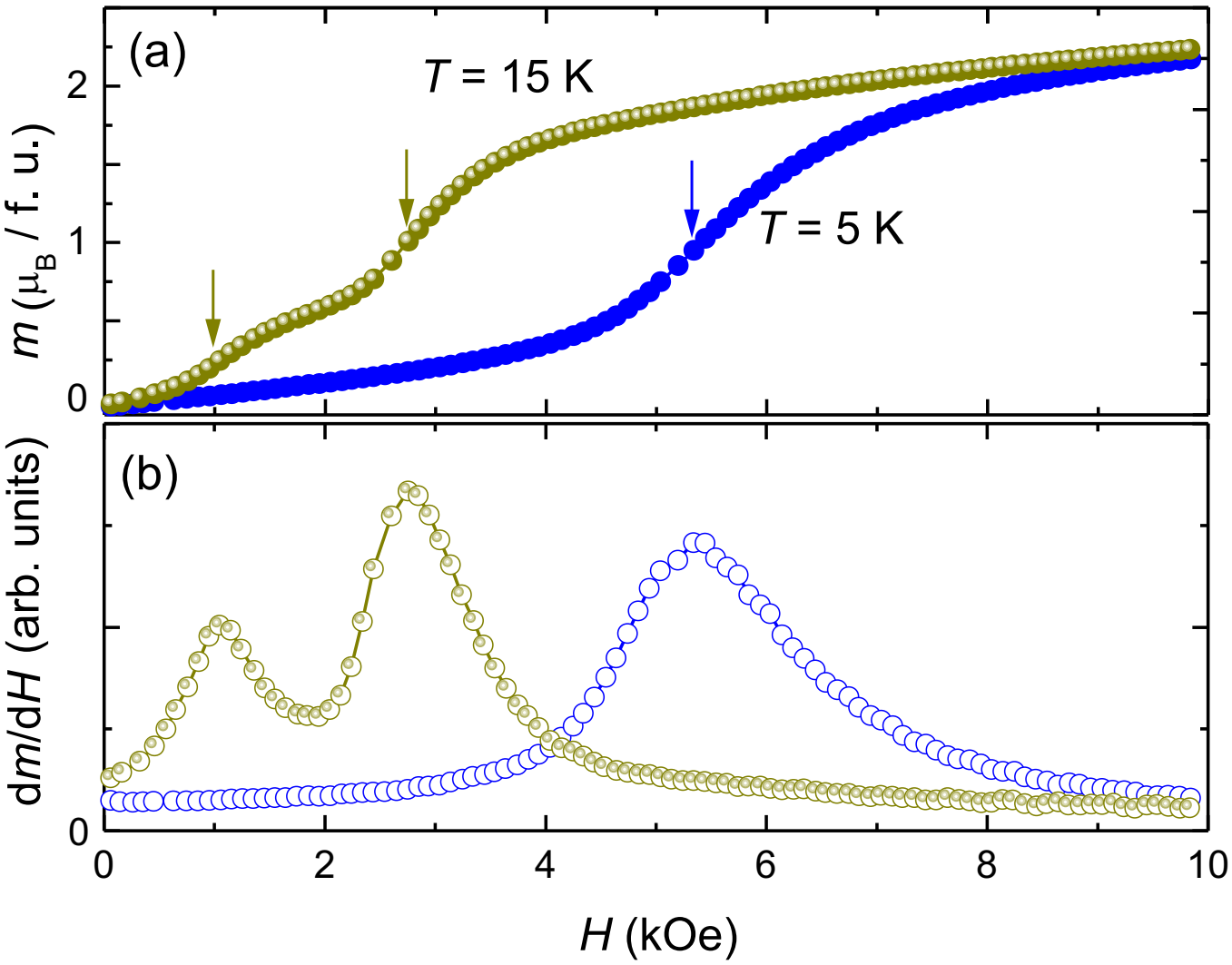

FIG. 4. (a) Initial magnetization m and (b) dc susceptibility dm/dH of HI90 at 5 K and 15 K. The critical fields H_{ac} are indicated by the arrows in (a).

respectively. It follows that the symmetry breaking occurs only for the Fe(III) moments which decouple from the Fe(II) sub-system at the critical field. During the metamagnetic transition subsequent to the symmetry breaking, major flipping of Fe(II) moments takes place as they are redirected along the external field. A drastic change at $T < 6$ K for the high-field transition is observed, which indicates that below this temperature the symmetry breaking and the metamagnetic transition occur simultaneously. Since symmetry breaking is caused by Fe(III) and metamagnetism by Fe(II), the simultaneous occurrence of these effects suggests that the two cation species are strongly coupled below $T < 6$ K. In this final stage of freezing the field-induced transition results in a ferrimagnetic arrangement, which is studied further below.

Figure 6 shows the magnetization loops $m(H)$ above and below T_f. All features of the magnetization loops, i.e. remanent moment m_R and coercive field H_C, start from low values at high temperature, $T > T_\mathrm{f}$, and increase exponentially with decreasing temperature, obeying a law $\propto e^{(-T/T_0)}$ (for H_C see inset in Fig. 6). This exponential behavior has also been observed in amorphous magnets, such as PdFeMn[43], Fe-Zr[44], and in rare-earth alloys[45,46]. Such behavior indicates that the thermodynamic evolution of hysteresis originates from intrinsic exchange interactions and not from thermally-activated domain-wall movement, which would be the case, if the coercivity obeyed a power

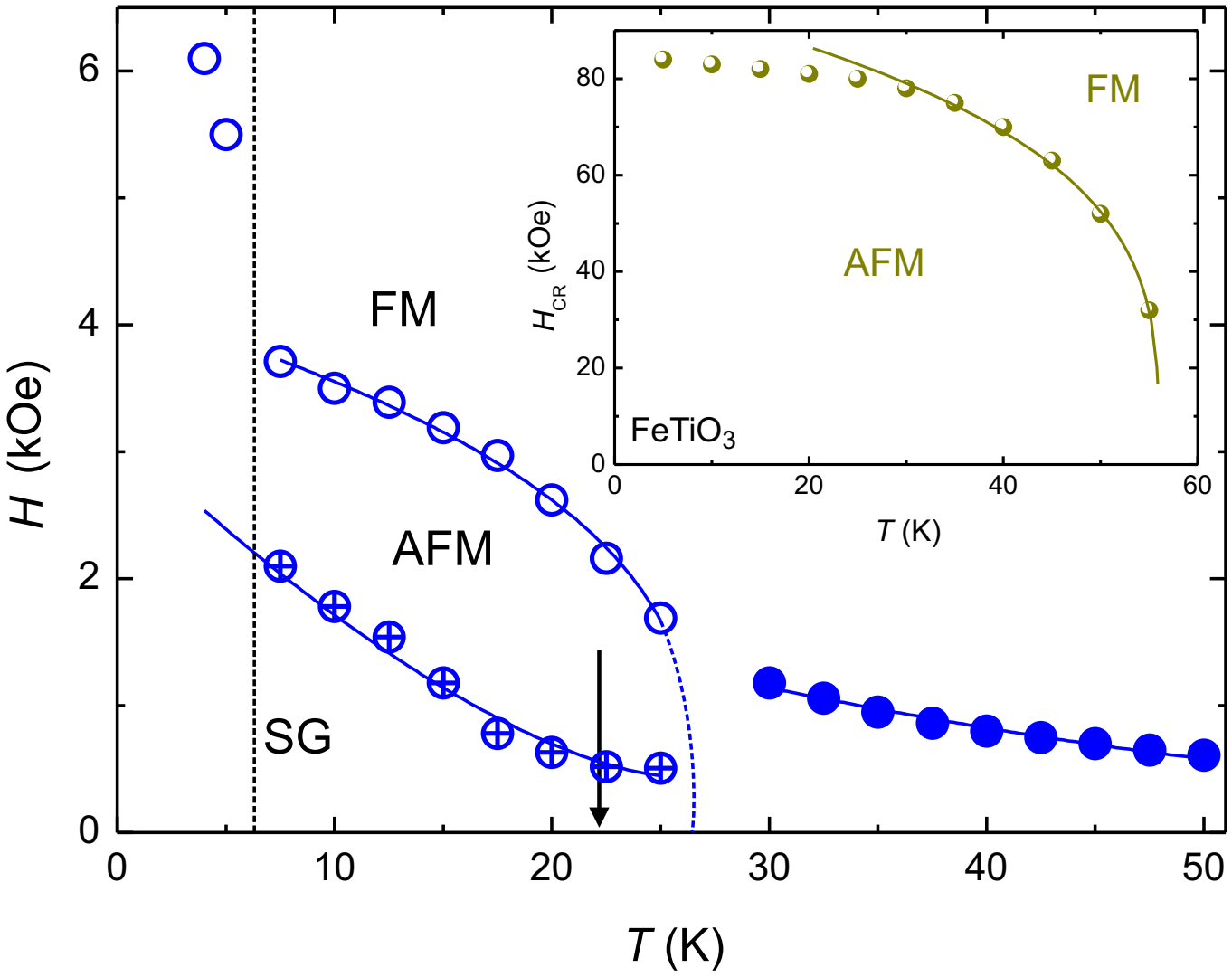

FIG. 5. $H-T$ phase diagram of HI90 showing the low-field (crossed circles) and the high-field (open circles) transitions. The inset shows the $H-T$ phase diagram of $FeTiO_3$, which indicates a metamagnetic transition. The arrow at $T = 22$ K indicates the location of T_f determined by extrapolation of the frequency-dependent *ac* susceptibility to $\omega = 0$.

law[47] $H_C(T)^{1/\beta} \propto T/T_C$. (This would represent the case when the mixed valence states are percolated). In the presence of interface exsolution patterns the Fe(II)-Fe(III) interactions would manifest as interface exchange bias[48,49]. As shown in the inset of Fig. 6 the magnetic moment does not saturate at low temperature, even at a field of 85 kOe. The moment reaches a pseudo-saturation at approximately 10 kOe and increases continuously with increasing applied field, revealing a paramagnetic-like behavior. The theoretical saturation moment m_{max} for a solid solution with composition x can be calculated using[50] $m_{max} = \sqrt{(2-2x)m^2_{Fe(III)} + (x)m^2_{Fe(II)}}$. According to Hund's rule we obtain the respective ionic moments as $m_{Fe(III)} = 5.92\mu_B$ and $m_{Fe(II)} = 4.90\mu_B$ using $S = 5/2$ for Fe(III) ($3d^5$), and $S = 4/2$ for Fe(II) ($3d^6$). This gives theoretical magnetic moments for the solid solution of $5.76\mu_B$ / f.u. for $x = 0.8$ (HI80) and $5.35\mu_B$ / f.u. for $x = 0.9$ (HI90), for all moments aligned parallel to the field. The continuous increase of the moment indicates enhanced unfolding of moments along the field. We can therefore make a rough estimation of the degree of polarization starting from 0 ($m_S = 0$) to 1 ($m_{eff} = m_{max}$). At a field of 85 kOe the moment lies at 3.4 μ_B/f.u, which suggests a polarization of more than 0.6. We therefore conclude that increasing the applied field generates spin flops, resulting in a continuous spin alignment along the field axis.

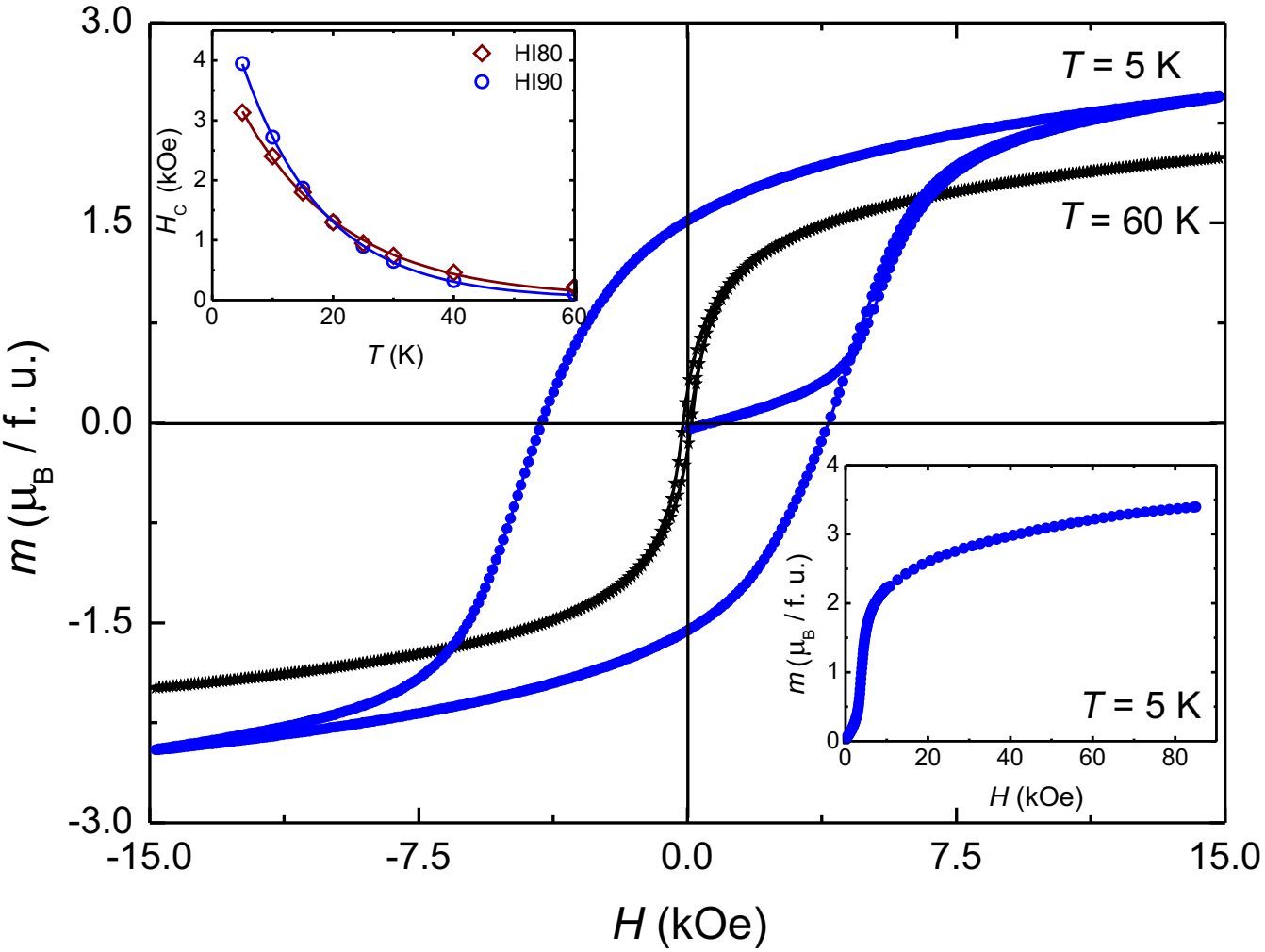

FIG. 6. Magnetization loops $m(H)$ of HI90 at $T = 5$ K and 60 K. Upper left inset shows the evolution of the coercive field H_c with decreasing temperature where the solid lines are fits using an exponential function. Lower right inset shows the high-field magnetization up to 85 kOe at 5 K.

V. CONCLUSIONS

We investigated the dynamics of freezing in the $(x)FeTiO_3$–$(1\text{-}x)Fe_2O_3$ system and found that it obeys a power law, indicative of critical slowing down. Samples with $x = 0.8$ and 0.9 behave like an Ising 3D spin glass with dynamic exponent $z\nu \approx 7$. The relaxation rates are quite slow (kHz-range) due to the collective flipping of superspins during thermal fluctuations. Moreover, there is no evidence of specific reentrant or cluster spin-glass characteristics in these samples. Magnetization curves in the frustrated phase reveal symmetry breaking from the spin-glass-like state to an intermediate state, followed by a subsequent metamagnetic transition similar to that of ilmenite. The critical field H_{cr} where symmetry breaking occurs denotes the AT line and obeys a $H \propto (1 - T/T_f)^{3/2}$ law. Increasing the *dc* field above the two transitions continuously flops spins along the field axis. Finally, the deeper understanding of spin-glass freezing as an intrinsic property has strong potential for aiding identification of hemo-ilmenite solid solutions in rock samples on the Earth and other planets.

ACKNOWLEDGMENTS

The authors would like to thank E. Fischer for his assistance with the sample preparation process and Marta-Dacil Rossell for her assistance with XRD experiments. This work was supported by the Swiss National Science Foundation

224 Grant No. 200021-121844.

* Corresponding author. Email: michalis.charilaou@erdw.ethz.ch
[1] C. A. M. Mulder, A. J. van Duyneveldt, and J. A. Mydosh, Phys. Rev. B **23**, 1384 (1981).
[2] S. Kirkpatrick, C. D. Gelatt, Jr., and M. P. Vecchi, Science **220**, 671 (1983).
[3] K. Binder and A. P. Young, Rev. Mod. Phys. **58**, 801 (1986).
[4] K.H. Fischer and J. A. Hertz, *Spin Glasses*, Cambridge University Press (1991).
[5] J. A. Mydosh, *Spin Glasses: An Experimental Introduction*. Taylor and Francis, London, 1993.
[6] G. Aeppli and P. Chandra, Science **275**, 177 (1997).
[7] S. A. McEnroe, P. Robinson, and P. Panish, Am. Mineral. **86**, 1447 (2001).
[8] S. A. McEnroe, R. J. Harrison, P. Robinson, and F. Langhorst, Geophys. J. Int. **151**, 890 (2002).
[9] P. Robinson, R. J. Harrison, S. A. McEnroe, and R. B. Hargraves, Nature **418**, 517 (2002).
[10] S. A. McEnroe, L. L. Brown, and P. Robinson, J. Appl. Geophys., **56**(3), 195 (2004).
[11] D. H. Lindsley, Carnegie Institution of Washington Yearbook **62**, 60 (1963).
[12] M. Charilaou, J. F. Löffler, and A. U. Gehring, Geophys. J. Int. **185**, 647 (2011).
[13] Y. Ishikawa, M. Arai, N. Saito, M. Kohgi, and H. Takei, J. Magn. Magn. Mater. **31**, 1381 (1983).
[14] Y. Ishikawa, N. Saito, M. Arai, Y. Watanabe, and H. Takei, J. Phys. Soc. Jpn. **54**, 312 (1985).
[15] M. Arai and Y. Ishikawa, J. Phys. Soc. Jpn., **54**, 795 (1985).
[16] M. Arai, Y. Ishikawa, N. Saito, and H. Takei, J. Phys. Soc. Jpn., **54**, 781 (1985).
[17] M. Arai, Y. Ishkawa, and H. Takei, J. Phys. Soc. Jpn., **54**, 2279 (1985).
[18] B. P. Burton, P. Robinson, S. A. McEnroe, K. Fabian, and T. B. Ballaran, Am. Mineral. **93**, 1260 (2008).
[19] A. U. Gehring, H. Fischer, E. Schill, J. Granwehr, and J. Luster, Geophys. J. Int. **169**, 917 (2007).
[20] A. U. Gehring, G. Mastrogiacomo, H. Fischer, P. G. Weidler, E. Müller, and J. Luster, J. Magn. Magn. Mater. **320**, 3307 (2008).
[21] R. J. Harrison, Geochem. Geophy. Geosy. **10**, Q02Z02 (2009).
[22] R. J. Harrison, S. A. T. Redfern, and R. I. Smith, Am. Mineral. **85**, 194 (2000).
[23] L. Navarrete, J. Dou, D. M. Allen, R. Schad, P. Padmini, P. Kale, and R. K. Pandey, J. Am. Ceram. Soc. **89**, 1601 (2006).
[24] C. Rüdt, P. J. Jensen, A. Scherz, J. Lindner, P. Poulopoulos, and K. Baberschke, Phys. Rev. B **69**, 014419 (2004).
[25] S. Prüfer and M. Ziese, Phys. Stat. Sol. (b), **245**, 1661 (2008).
[26] P. C. Hohenberg and P. I. Halperin, Rev. Mod. Phys. **49**, 435 (1977).
[27] K. Binder and A. P. Young, Phys. Rev. B, **29**, 2864 (1984).
[28] J. Souletie and J. L. Tholence, Phys. Rev. B **32**, 516 (1985).
[29] A. T. Ogielski and I. Morgenstern, Phys. Rev. Lett. **54**, 928 (1985); J. Appl. Phys. **57**, 3382 (1985).
[30] C. Djurberg, P. Svedlindh, P. Nordblad, M. F. Hansen, F. Bødker, and S. Mørup, Phys. Rev. Lett. **79**, 5154 (1997).
[31] A. Mauger, J. Ferrè, M. Ayadi, and P. Nordblad, Phys. Rev. B **37**, 9022 (1988).
[32] J. R. L. de Almeida and D. J. Thouless, J. Phys. A: Math. Gen. **11**, 983 (1978).
[33] P. A. Young, Comput. Phys. Commun. **169**, 144 (2005).
[34] A. P. Young, J. Magn. Magn. Mater. **310**, 1482 (2007); J. Phys. Conference Series **95**, 012003 (2008).
[35] Y. Takano, A. Arai, Y. Takahashi, K. Takase, and K. Sekizawa, J. Appl. Phys. **93**, 8197 (2003).
[36] J. Mattsson, T. Jonsson, P. Nordblad, H. Aruga Katori, and A. Ito, Phys. Rev. Lett. **74**, 4305 (1995).
[37] More information available at Quantum Design: http://www.qdusa.com
[38] N. E. Brown, A. Navrotsky, G. L. Nord, and S. K. Banerjee, Am. Mineral. **78** 941 (1993).
[39] S. Nakamae, Y. Tahri, C. Thibierge, D. L´ Hôte, E. Vincent, V. Dupuis, E. Dubois, and R. Perzynski, J. Appl. Phys. **105**, 07E318 (2009).
[40] A. Ito, H. Aruga, E. Torikai, M. Kikuchi, Y. Syono, and H. Takei, Phys. Rev. Lett. **57**, 483 (1986).
[41] H. Kato, M. Yamada, H. Yamauchi, H. Hiroyoshi, H. Takei, and H. Watanabe, J. Phys. Soc. Jpn. **51**, 1769 (1982).
[42] C. Frandsen, B. P. Burton, H. K. Rasmussen, S. A. McEnroe, and S. Morup, Phys. Rev. B **81**, 224423 (2010).
[43] D. W. Carnegie, Jr. and H. Claus, Phys. Rev. B **20**, 1280 (1979).
[44] D. A. Read, T. Moyo and G. C. Hallam, J. Magn. Magn. Mater. **44**, 279 (1984).
[45] K. H. J. Buschow and A. M. van der Kraan, J. Magn. Magn. Mat. **22**, 220 (1981).
[46] S. Mukherjee, R. Ranganathan, and P. Mondal, J. Phys. Chem. Solids **61**, 1433 (2000).
[47] J. I. Arnaudas, A. Del Moral, and P. A. J. De Groot, J. Magn. Magn. Mater. **104-107**, 115 (1992).
[48] R. J. Harrison, S. A. McEnroe, P. Robinson, B. Carter-Stiglitz, E. J. Palin, and T. Kasama, Phys. Rev. B, **76**, 174436 (2007).
[49] H. S. Nabi, R. J. Harrison, and R. Pentcheva, Phys. Rev. B **81**, 214432 (2010).
[50] F. Millange, S. de Brion, and G. Chouteau, Phys. Rev. B **62**, 5619 (2000).